

Sound propagation over the ground with a random spatially-varying surface admittance

Didier Dagna^{a)} and Philippe Blanc-Benon

Univ Lyon, École Centrale de Lyon, Laboratoire de Mécanique des Fluides et d'Acoustique, UMR CNRS 5509, F-69134 Écully, France

(Received 28 February 2017; revised 21 September 2017; accepted 22 September 2017; published online 13 October 2017)

Sound propagation over the ground with a random spatially-varying surface admittance is investigated. Starting from the Green's theorem, a Dyson equation is derived for the coherent acoustic pressure. Under the Bourret approximation, an explicit expression is deduced and an effective admittance that depends on the correlation function of the admittance fluctuations is exhibited. An asymptotic expression at long range is then obtained. Influence of the randomness on the amplitude of the reflection coefficient and on the wavenumbers of the surface wave component is analyzed. Afterwards, numerical simulations of the linearized Euler equations are carried out and the coherent pressure obtained by an ensemble-averaging over 200 realizations of the admittance is found to be in good agreement with the analytical solution. In the considered examples of grounds, the mean intensity is shown to be similar to the intensity in the non-random case, except near interferences that are smoothed out due to randomness. It is however exemplified that the intensity fluctuations can be large, especially near destructive interferences. © 2017 Acoustical Society of America.

<https://doi.org/10.1121/1.5006180>

[VEO]

Pages: 2058–2072

I. INTRODUCTION

Predicting outdoor sound propagation at long range remains a tough challenge. Recent developments in numerical methods have allowed to consider more and more complex wave effects (see, e.g., Refs. 1–4). Numerical solutions of the parabolic or linearized Euler equations have proved to compare favorably with measured acoustical fields in realistic environments with mixed grounds, non-flat terrain and inhomogeneous atmosphere, e.g., Refs. 5 and 6. Nevertheless, the input parameters of these high-fidelity simulations are required to be sufficiently accurate in order to obtain reliable output data, which is not always possible. For instance, a precise knowledge of the state of the atmosphere is impracticable, due to the inherent randomness of turbulence, among other reasons. This leads therefore to uncertainties in the sound pressure level (SPL), as discussed, e.g., in Refs. 4 and 7.

Sources of uncertainties in the acoustic properties of ground surfaces are also numerous. First, these are related to the current measurements methods, which are based in a large majority on the two-microphone or transfer function method.^{8–11} A possible mismatch in gain or phase between the microphones or uncertainties in the exact position of the source or the microphones would lead to uncertainties in the transfer function and hence the surface impedance.⁹ Moreover, the parameters of an impedance model, instead of the impedance itself, are often deduced from the measurements of the transfer function. Depending on the choice of the model, predicted SPL at long range can be significantly different.¹⁰ Second, the impedance measurements are local in time and space. However, the surface ground properties

vary according to the time-of-the-day, as they depend for instance on the soil moisture.¹² The monthly or seasonal variations are also important, which has been shown for instance in the measurements reported by Gauvreau.¹³ The time variations of surface impedance must therefore be accounted for in predictions of long-term SPLs. Besides, even if a ground surface is apparently uniform, its acoustic properties can have large spatial variations. This was recently highlighted by Guillaume *et al.*¹¹ who have determined the parameters of a surface impedance model along 50 m lines at measurement points spaced by 3 m and for several ground types. The spatial variations were significant as the normalized standard deviations were between 5% and 30%. The corresponding variation for the admittance and impedance was about 10% for synthetic surfaces and between 10% and 40% for natural grounds.

Consequence of the uncertainties in the ground properties on the SPL predictions has been partly investigated. Ostashev *et al.*¹⁴ have treated the case of a homogeneous admittance plane with random properties. After prescribing probability density functions for the flow resistivity, tortuosity, and porosity of the ground surface, the statistics of the sound pressure at long range were computed using the analytical solution for a homogeneous plane. The main results of their study are first that the mean intensity, which corresponds to the mean SPL, is almost identical to the intensity obtained for the mean value of the ground characteristics, and second that the standard deviation of the intensity fluctuations increases with the distance, meaning that for a particular realization of the ground parameters, larger deviations of the SPL from the mean value can be obtained as the range increases. The influence of random spatial variations of the ground properties was first treated by Watson and Keller.^{15,16} The authors consider four

^{a)}Electronic mail: didier.dagna@ec-lyon.fr

types of boundaries, and among them a spatially-varying admittance plane. In Ref. 15, they obtain analytical expressions for the first two statistical moments, based on the regular perturbation method. In particular, a mean reflection coefficient was determined and an effective admittance, which depends on the admittance spatial correlation function, was obtained. In Ref. 16, they investigate the same problems using another perturbation method; namely, the smoothing method. In both papers, the unperturbed solution is that for a zero-mean admittance plane, which is a crude approximation for ground surfaces. More recently, Guillaume *et al.*¹¹ have also examined the influence of spatial variations of the surface impedance. Based on their measurements, they have compared SPL predictions for a homogeneous ground using measured mean values of the grounds parameters to those using these mean values plus or minus the measured standard deviations. At middle and long ranges, SPLs were almost the same for the synthetic surface, while for natural grounds, the variability was significant for frequencies below 600 Hz with deviations that can reach 10 dB.

The objectives of the paper are twofold: (1) to extend the analytical solution for the mean pressure for a ground with a spatially-varying admittance obtained by Watson and Keller, and (2) to investigate the intensity fluctuations and compare them to those obtained for a ground with a homogeneous random admittance.

The paper is organized as follows. In Sec. II, an analytical solution for the mean acoustic pressure over the ground with a random spatially-varying admittance is derived and an asymptotic expression is obtained in the far field. An effective admittance is deduced and its variation with the correlation length and standard deviation of the admittance fluctuations is discussed. In Sec. III, numerical simulations, based on the resolution of the linearized Euler equations in the time domain, are carried out. The mean pressure computed from ensemble-averaging over 200 realizations of the random admittance is compared to the analytical solution. Finally, the mean intensity and intensity fluctuations are investigated.

II. MEAN ACOUSTIC FIELD AND EFFECTIVE ADMITTANCE

A. Integral formulation for the Green's function

The study is concerned with the propagation of acoustic waves over the ground with a random spatially-varying admittance. This implies that the spatial variations of the admittance are not known, but that some statistical properties of these variations are available. The solution for a realization of the spatially-varying admittance is therefore not of interest hereafter, but the statistical properties of the sound pressure field are investigated.

The scheme of the problem is depicted in Fig. 1. For the sake of simplicity, we consider a two-dimensional (2D) problem and we denote by $\mathbf{r} = (x, z)$ the Cartesian coordinates. The acoustic field is generated by a point source of angular frequency ω . The acoustic wave number is $k_0 = \omega/c_0$, where $c_0 = 340 \text{ m s}^{-1}$ is the sound speed. The source and the receiver are located, respectively, at $\mathbf{r}_0 = (x_0, z_0)$ and $\mathbf{r} = (x, z)$. The ground is characterized by its normalized spatially-varying admittance $\beta(x)$. We denote by $\langle \dots \rangle$ the

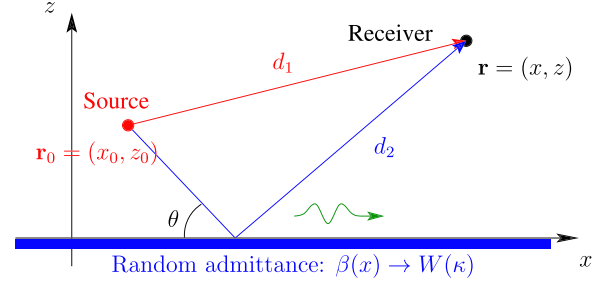


FIG. 1. (Color online) Propagation of acoustic waves over the ground with a spatially-varying surface admittance.

average operator over an ensemble of realizations of $\beta(x)$ and we assume that the average admittance $\langle \beta \rangle$ is constant. The admittance is split into $\beta(x) = \langle \beta \rangle + \beta'(x)$, where $\beta'(x)$ is the fluctuating admittance. By definition, $\langle \beta'(x) \rangle = 0$.

One introduces the Green's function G of the perturbed problem, which is the scattering of acoustic waves by an inhomogeneous ground of admittance $\beta(x)$. It satisfies the Helmholtz equation:

$$(\Delta + k_0^2)G(\mathbf{r}, \mathbf{r}_0) = \delta(\mathbf{r} - \mathbf{r}_0), \quad (1)$$

where δ is the Dirac delta function and Δ is the Laplace operator, along with the boundary condition at the plane $z = 0$,

$$\left(\frac{\partial}{\partial z} + ik_0\beta(x) \right) G(x, z = 0, \mathbf{r}_0) = 0. \quad (2)$$

In addition, one introduces the Green's function G_0 of the unperturbed problem, which is the scattering of acoustic waves by a homogeneous ground of admittance $\langle \beta \rangle$. It also satisfies the Helmholtz equation

$$(\Delta + k_0^2)G_0(\mathbf{r}, \mathbf{r}_0) = \delta(\mathbf{r} - \mathbf{r}_0), \quad (3)$$

but with the boundary condition at the ground $z = 0$

$$\left(\frac{\partial}{\partial z} + ik_0\langle \beta \rangle \right) G_0(x, z = 0, \mathbf{r}_0) = 0. \quad (4)$$

Applying the Green's theorem:

$$\int_V [G\Delta G_0 - G_0\Delta G]dV = \int_S \left(G \frac{\partial G_0}{\partial n} - G_0 \frac{\partial G}{\partial n} \right) dS \quad (5)$$

over the half-space $z \geq 0$, one gets the integral equation

$$G(\mathbf{r}, \mathbf{r}_0) = G_0(\mathbf{r}, \mathbf{r}_0) + \int_{-\infty}^{\infty} G_0(\mathbf{r}, \mathbf{r}_1)V(x_1)G(\mathbf{r}_1, \mathbf{r}_0)dx_1, \quad (6)$$

with the random surface potential $V(x_1) = -ik_0\beta'(x_1)$. This equation has been obtained previously by Chandler-Wilde and Hothersall [Eq. (6) of Ref. 17].

B. Analytical solution in the Fourier space

In this section, an analytical expression is sought for the average or coherent Green's function, denoted thereafter by

$\langle G \rangle$. With this purpose, a standard method to treat wave propagation in random media or above random boundaries, namely, the diagram technique (see, e.g., Refs. 18–20), is employed. In acoustics, it has been used formerly to derive the average sound field or effective media quantities for multiple scattering problems, such as the propagation through a turbulent medium⁴ or through a layer of scatterers.²¹ Recently, based on this approach, Faure *et al.*²² have proposed an effective admittance to represent the reflection over rough surfaces.

Following Ishimaru *et al.*,²³ it can be shown from Eq. (6) that $\langle G \rangle$ satisfies the Dyson equation,

$$\langle G(\mathbf{r}, \mathbf{r}_0) \rangle = G_0(\mathbf{r}, \mathbf{r}_0) + \iint_{-\infty}^{\infty} G_0(\mathbf{r}, \mathbf{r}_1) M(\mathbf{r}_1, \mathbf{r}_2) \times \langle G(\mathbf{r}_2, \mathbf{r}_0) \rangle d\mathbf{x}_1 d\mathbf{x}_2, \quad (7)$$

where $\mathbf{r}_1 = (x_1, z_1 = 0)$ and $\mathbf{r}_2 = (x_2, z_2 = 0)$ are two points at the ground surface and the operator M is referred to as the mass or self-energy operator in the literature. It corresponds to the summation of all possible connected diagrams contributing to $\langle G \rangle$.¹⁸ The mass operator is generally not explicitly known, and it must be approximated in order to get an analytical expression for the mean field. The usual approximation, called the Bourret approximation, is to keep only the first term of the mass operator,

$$M(\mathbf{r}_1, \mathbf{r}_2) \approx \langle V(x_1) G_0(\mathbf{r}_1, \mathbf{r}_2) V(x_2) \rangle = -k_0^2 \langle \beta'(x_1) \beta'(x_2) \rangle G_0(\mathbf{r}_1, \mathbf{r}_2). \quad (8)$$

The diagrammatic form of the Dyson equation with the exact mass operator and with the Bourret approximation is shown in Fig. 2. The range of validity of the Bourret approximation is discussed in Appendix B. Denoting, respectively, by $\sigma_\beta = \sqrt{\langle \beta'^2 \rangle}$ and by L the standard deviation (std) and the correlation length of the admittance fluctuations, a necessary condition in the long-wavelength limit ($k_0 L \ll 1$) is $|\sigma_\beta|^2 k_0 L \ll 1$. In the short-wavelength limit ($k_0 L \gg 1$), it is required that $|\sigma_\beta|^2 \ll \text{Re}[\langle \beta \rangle]^2$ if $\text{Im}[\langle \beta \rangle] \leq 0$ and $|\sigma_\beta|^2 \ll |\langle \beta \rangle|^2$ if $\text{Im}[\langle \beta \rangle] \geq 0$.

Under the Bourret approximation, the Dyson equation is written as

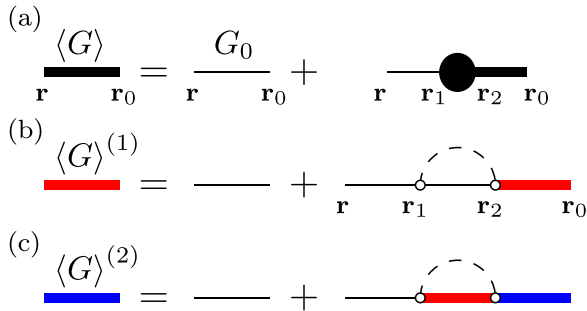


FIG. 2. (Color online) Diagrammatic form of the Dyson equation (a) using the exact mass operator [Eq. (7)], (b) the Bourret approximation [Eq. (9)], and (c) the next approximation of the mass operator. The latter is used in Appendix B to investigate the range of applicability of the Bourret approximation.

$$\langle G(\mathbf{r}, \mathbf{r}_0) \rangle = G_0(\mathbf{r}, \mathbf{r}_0) - k_0^2 \iint_{-\infty}^{\infty} G_0(\mathbf{r}, \mathbf{r}_1) \langle \beta'(x_1) \beta'(x_2) \rangle \times G_0(\mathbf{r}_1, \mathbf{r}_2) \langle G(\mathbf{r}_2, \mathbf{r}_0) \rangle d\mathbf{x}_1 d\mathbf{x}_2. \quad (9)$$

Thereafter, the admittance distribution is assumed to be statistically homogeneous, so that the correlation function $\langle \beta'(x_1) \beta'(x_2) \rangle$ depends only on the spatial distance $x_1 - x_2$. As a consequence, the statistics of the acoustic field are invariant under arbitrary horizontal translation of the source-receiver pair. In particular, the average Green's function satisfies the property $\langle G(\mathbf{r}, \mathbf{r}_0) \rangle = \langle G(x - x_0, z, z_0) \rangle$. The Fourier transform along the x -direction of the average Green's function can therefore be expressed as

$$\int_{-\infty}^{\infty} \langle G(\mathbf{r}, \mathbf{r}_0) \rangle e^{-ikx} dx = \langle \hat{G}(\kappa, z, z_0) \rangle e^{-ikx_0}. \quad (10)$$

After some calculations detailed in Appendix A, applying the Fourier transform to Eq. (9) gives

$$\langle \hat{G}(\kappa, z, z_0) \rangle = \hat{G}_0(\kappa, z, z_0) - \frac{k_0^2}{2\pi} \hat{G}_0(\kappa, z, z_1) \langle \hat{G}(\kappa, z_2, z_0) \rangle \times \int_{-\infty}^{\infty} W(\kappa') \hat{G}_0(\kappa - \kappa', z_1, z_2) d\kappa', \quad (11)$$

where \hat{G}_0 is the Fourier transform of the Green's function for the unperturbed problem

$$\hat{G}_0(\kappa, z, z_0) = \frac{1}{2i\alpha} \left[e^{i\alpha|z-z_0|} + R_0(\kappa) e^{i\alpha(z+z_0)} \right], \quad (12)$$

with the vertical wavenumber $\alpha = \sqrt{k_0^2 - \kappa^2}$ and the reflection coefficient

$$R_0(\kappa) = \frac{\alpha - k_0 \langle \beta \rangle}{\alpha + k_0 \langle \beta \rangle}, \quad (13)$$

and W is the Fourier transform of the correlation function

$$W(\kappa) = \int_{-\infty}^{\infty} \langle \beta'(x) \beta'(x+r) \rangle e^{-i\kappa r} dr. \quad (14)$$

In order to compare the solution for a ground with a random admittance to the solution for a ground with a constant admittance, the average Green's function $\langle \hat{G}(\kappa, z, z_0) \rangle$ is rewritten under the form

$$\langle \hat{G}(\kappa, z, z_0) \rangle = \frac{1}{2i\alpha} \left[e^{i\alpha|z-z_0|} + R_{\text{eff}}(\kappa) e^{i\alpha(z+z_0)} \right], \quad (15)$$

where R_{eff} can be interpreted as an effective reflection coefficient of the random surface. Inserting Eq. (15) in Eq. (11) leads to

$$R_{\text{eff}}(\kappa) = R_0(\kappa) - \frac{k_0^2}{2\pi} \frac{1}{2i\alpha} [1 + R_0(\kappa)] [1 + R_{\text{eff}}(\kappa)] \times \int_{-\infty}^{\infty} \frac{W(\kappa')}{2i\alpha(\kappa - \kappa')} [1 + R_0(\kappa - \kappa')] d\kappa',$$

which can be written as

$$R_{\text{eff}}(\kappa) = R_0(\kappa) + \frac{k_0^2}{2\pi} \frac{1}{\alpha + k_0 \langle \beta \rangle} [1 + R_{\text{eff}}(\kappa)] \times \int_{-\infty}^{\infty} \frac{W(\kappa')}{\alpha(\kappa - \kappa') + k_0 \langle \beta \rangle} d\kappa'.$$

Introducing the classical form for the reflection coefficient for a ground with a constant admittance

$$R_{\text{eff}}(\kappa) = \frac{\alpha - k_0 \beta_{\text{eff}}(\kappa)}{\alpha + k_0 \beta_{\text{eff}}(\kappa)}, \quad (16)$$

the effective admittance $\beta_{\text{eff}}(\kappa)$ is given by

$$\beta_{\text{eff}}(\kappa) = \langle \beta \rangle - \frac{k_0}{2\pi} \int_{-\infty}^{\infty} \frac{W(\kappa - \kappa')}{\alpha(\kappa') + k_0 \langle \beta \rangle} d\kappa'. \quad (17)$$

It should be noticed, that for $\langle \beta \rangle = 0$, we retrieve the expressions of the effective admittance obtained by Watson and Keller [Eq. (43) of Ref. 15 and Eq. (23c) of Ref. 16]. For $\langle \beta \rangle \neq 0$, they however differ because we do not consider the same unperturbed problem. In the papers of Watson and Keller, it corresponds to the propagation above a homogeneous ground with zero mean admittance while we consider the more general case of a homogeneous ground with non-zero mean admittance.

C. Far-field asymptotic analysis

The mean acoustic pressure can then be obtained by the inverse Fourier transform

$$\langle G(\mathbf{r}, \mathbf{r}_0) \rangle = \frac{1}{2\pi} \int_{-\infty}^{\infty} \langle \hat{G}(\kappa, z, z_0) \rangle e^{i\kappa(x-x_0)} d\kappa. \quad (18)$$

However, its computation can be cumbersome, as it requires the evaluation of an integral whose integrand is oscillatory. Usually, for long-range applications, asymptotic expression of such integral is sought using the method of steepest descent.²⁴⁻²⁶

The acoustic pressure in Eq. (15) is first split into a direct wave $\langle \hat{G}(\kappa, z, z_0) \rangle_D$ and a reflected wave $\langle \hat{G}(\kappa, z, z_0) \rangle_R$, with

$$\langle \hat{G}(\kappa, z, z_0) \rangle_D = \frac{1}{2i\alpha} e^{i\alpha|z-z_0|},$$

$$\langle \hat{G}(\kappa, z, z_0) \rangle_R = \frac{1}{2i\alpha} R_{\text{eff}}(\kappa) e^{i\alpha(z+z_0)}.$$

The direct wave contribution is well-known and corresponds to the Green's function in free-space

$$\langle G(\mathbf{r}, \mathbf{r}_0) \rangle_D = \frac{1}{2\pi} \int_{-\infty}^{\infty} \langle \hat{G}(\kappa, z, z_0) \rangle_D e^{i\kappa(x-x_0)} d\kappa = -\frac{i}{4} H_0^{(1)}(k_0 |\mathbf{r} - \mathbf{r}_0|),$$

where $H_0^{(1)}$ is the Hankel function of the first kind. Its asymptotic expression at long range $k_0 d_1 \gg 1$, with $d_1 = \sqrt{(x-x_0)^2 + (z-z_0)^2}$ is given by

$$\langle G(\mathbf{r}, \mathbf{r}_0) \rangle_D \approx \frac{1}{4i} \sqrt{\frac{2}{\pi}} \frac{1}{\sqrt{i k_0 d_1}} e^{i k_0 d_1}. \quad (19)$$

The reflected wave is written in the physical space as

$$\langle G(\mathbf{r}, \mathbf{r}_0) \rangle_R = \frac{1}{2\pi} \int_{-\infty}^{\infty} \langle \hat{G}(\kappa, z, z_0) \rangle_R e^{i\kappa(x-x_0)} d\kappa = \frac{1}{2\pi} \int_{-\infty}^{\infty} \frac{1}{2i\alpha} R_{\text{eff}}(\kappa) e^{i\kappa(x-x_0) + i\alpha(z+z_0)} d\kappa. \quad (20)$$

In order to apply the method of steepest descent, the integrand must be first extended in the complex plane. Special attention must be paid to the function $\alpha(\kappa)$, as it is multivalued, and so is $\beta_{\text{eff}}(\kappa)$. The usual choice for this problem is to define $\alpha(\kappa) = i \text{pv} \sqrt{-i(\kappa + k_0)} \text{pv} \sqrt{i(\kappa - k_0)}$, where $\text{pv} \sqrt{\dots}$ is the principal value of the square root function, which is generally implemented in numerical computing applications such as MATLAB. The saddle points of the phase function $Q(\kappa) = i\kappa(x-x_0) + i\alpha(z+z_0)$, which are the points for which $dQ/d\kappa = 0$, can then be determined in the complex κ -plane. In this case, there is only one saddle point located at $(\kappa_s = k_0 \cos \theta, \alpha_s = k_0 \sin \theta)$, with $\cos \theta = (x-x_0)/d_2$, $\sin \theta = (z+z_0)/d_2$ and $d_2 = \sqrt{(x-x_0)^2 + (z+z_0)^2}$ and $Q(\kappa_s) = i k_0 d_2$. The steepest descent path is given by the equation $Q(\kappa) = Q(\kappa_s) - k_0 d_2 q^2$, with $-\infty < q < \infty$. The values of the horizontal and vertical wavenumbers along the steepest descent path are obtained by inverting the preceding equation, yielding

$$\kappa_{\text{sd}}(q) = k_0 \cos \theta (1 + iq^2) - iq k_0 \sin \theta \sqrt{2i - q^2},$$

$$\alpha_{\text{sd}}(q) = k_0 \sin \theta (1 + iq^2) + iq k_0 \cos \theta \sqrt{2i - q^2}.$$

The integration contour is then deformed onto the steepest descent path, as illustrated in Fig. 3. Applying the Cauchy theorem, one should be careful at the integrand singularities. With the chosen definition of $\alpha(\kappa)$, the steepest descent path does not cross the branch cuts of $\alpha(\kappa)$. Therefore, additional contributions can only come from singularities of the reflection coefficient. It is assumed thereafter that $W(\kappa)$ can be extended analytically in the complex plane (this is the case, for instance, for the Gaussian correlation function) so that $\beta_{\text{eff}}(\kappa)$ given by Eq. (17) is regular. Finally, the only singularities of the integrand are possible poles κ_p of the reflection coefficient, which satisfy the equation

$$D(\kappa_p) = \alpha(\kappa_p) + k_0 \beta_{\text{eff}}(\kappa_p) = 0. \quad (21)$$

This is an integral equation, that cannot be solved explicitly in the general case.

In the following, the study is limited to the long-wavelength limit ($k_0 L \ll 1$). The short-wavelength case ($k_0 L \gg 1$) is treated in Appendix D. In accordance with the range of application of the Bourret approximation, one assumes that $|\sigma_\beta|$ is not too large. Therefore, it is expected that there is still one pole, which lies close to the pole of the reflection coefficient for a ground with a homogeneous admittance

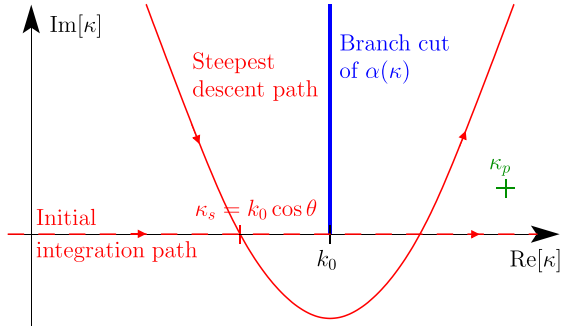


FIG. 3. (Color online) Deformation of the initial integration path for $\langle G(\mathbf{r}, \mathbf{r}_0) \rangle_R$ onto the steepest descent path in the complex κ -plane.

$\langle \beta \rangle (\kappa_p^0 = k_0 \sqrt{1 - \langle \beta \rangle^2})$ or at least, that the other poles are located far from the real axis so that their contributions are negligible. Under this assumption, the reflected wave is thus given by

$$\langle G(\mathbf{r}, \mathbf{r}_0) \rangle_R = \langle G(\mathbf{r}, \mathbf{r}_0) \rangle_{R, \text{sd}} + \langle G(\mathbf{r}, \mathbf{r}_0) \rangle_S.$$

The first term $\langle G(\mathbf{r}, \mathbf{r}_0) \rangle_{R, \text{sd}}$ denotes the steepest descent path contribution

$$\langle G(\mathbf{r}, \mathbf{r}_0) \rangle_{R, \text{sd}} = \int_{-\infty}^{\infty} F(q) e^{ik_0 d_2 - k_0 d_2 q^2} dq, \quad (22)$$

with

$$\begin{aligned} F &= \frac{1}{2\pi} \frac{1}{2i\alpha_{\text{sd}}} R_{\text{eff}}(\kappa_{\text{sd}}) \frac{d\kappa_{\text{sd}}}{dq} \\ &= \frac{1}{2\pi} \frac{1}{2i\alpha_{\text{sd}}} R_{\text{eff}}(\kappa_{\text{sd}}) \frac{2\alpha_{\text{sd}}}{\sqrt{2i - q^2}} \\ &= \frac{1}{2\pi i} R_{\text{eff}}(\kappa_{\text{sd}}) \frac{1}{\sqrt{2i - q^2}}. \end{aligned}$$

The second term $\langle G(\mathbf{r}, \mathbf{r}_0) \rangle_S$ is the surface wave contribution, given by

$$\langle G(\mathbf{r}, \mathbf{r}_0) \rangle_S = 2\pi i \text{Res}(\kappa_p) H[-\text{Im}(q_p)], \quad (23)$$

where H is the Heaviside function, $\text{Res}(\kappa_p)$ is the residue at the pole κ_p

$$\begin{aligned} \text{Res}(\kappa_p) &= \lim_{\kappa \rightarrow \kappa_p} \left[(\kappa - \kappa_p) \frac{1}{2\pi 2i\alpha} R_{\text{eff}}(\kappa) e^{i\kappa(x-x_0) + i\alpha(z+z_0)} \right] \\ &= \frac{1}{2\pi 2i\alpha_p} \lim_{\kappa \rightarrow \kappa_p} [(\kappa - \kappa_p) R_{\text{eff}}(\kappa)] e^{i\kappa_p(x-x_0) + i\alpha_p(z+z_0)} \end{aligned}$$

with $\alpha_p = \alpha(\kappa_p)$ and q_p is the numerical distance

$$q_p = \sqrt{i - i\kappa_p/k_0 \cos \theta - i\alpha_p/k_0 \sin \theta}.$$

The residue at the pole is given by

$$\text{Res}(\kappa_p) = a e^{i\kappa_p(x-x_0) + i\alpha_p(z+z_0)}, \quad (24)$$

with

$$a = \frac{1}{2\pi i} \frac{k_0 \beta_{\text{eff}}(\kappa_p)}{\kappa_p + k_0^2 \beta'_{\text{eff}}(\kappa_p) \beta_{\text{eff}}(\kappa_p)}, \quad (25)$$

and $\beta'_{\text{eff}}(\kappa_p) = d\beta_{\text{eff}}/d\kappa(\kappa_p)$. For a ground with a homogeneous admittance for which $\beta' = 0$, the equation above yields the classical formula for the residue at the pole.

To obtain an explicit asymptotic expression, the next step is to expand the function F in the integrand of Eq. (22) around $q=0$. However, due to the pole of the reflection coefficient, F is singular at $q=q_p$. If q_p is close to 0, corresponding to the pole located close to the saddle point in the κ -plane, the radius of convergence of the series would be dramatically limited. A uniform asymptotic expression can however be obtained using the method of pole subtraction. The principle of the method is to remove explicitly the singularity from the integrand. For that, one considers

$$\begin{aligned} \langle G(\mathbf{r}, \mathbf{r}_0) \rangle_{R, \text{sd}} &= \int_{-\infty}^{\infty} F_1(q) e^{-k_0 d_2 q^2} dq e^{ik_0 d_2} \\ &\quad + \int_{-\infty}^{\infty} \frac{a}{q - q_p} e^{-k_0 d_2 q^2} dq e^{ik_0 d_2}, \quad (26) \end{aligned}$$

with

$$F_1(q) = F(q) - \frac{a}{q - q_p}.$$

The last integral in Eq. (26) can be written as²⁵

$$\begin{aligned} \int_{-\infty}^{\infty} \frac{a}{q - q_p} e^{-k_0 d_2 q^2} dq &= a i \pi e^{-n^2} \\ &\quad \times [\text{erfc}(-in) - 2H[-\text{Im}(q_p)]], \end{aligned}$$

where $n = \sqrt{k_0 d_2} q_p$ is referred to as the numerical distance. The asymptotic expression of the first integral term in Eq. (26) can now be obtained. For $k_0 d_2 \gg 1$, only small values of q will contribute to this integral. Therefore, the first integral in Eq. (26) is made explicit by approximating $F_1(q)$ at the zeroth order

$$F_1(q=0) = \frac{1}{2i\pi} R_{\text{eff}}(\kappa_s) \frac{1}{\sqrt{2i}} + \frac{a}{q_p},$$

with the value of the reflection coefficient at the saddle point

$$R_{\text{eff}}(\kappa_s) = \frac{\sin \theta - \beta_{\text{eff}}(k_0 \cos \theta)}{\sin \theta + \beta_{\text{eff}}(k_0 \cos \theta)}. \quad (27)$$

Finally, the reflected wave in the physical space for large $k_0 r$ is given by

$$\begin{aligned} \langle G(\mathbf{r}, \mathbf{r}_0) \rangle_R &= \left[\frac{1}{2i\pi} R_{\text{eff}}(\kappa_s) \frac{1}{\sqrt{2i}} \sqrt{\frac{\pi}{k_0 d_2}} \right. \\ &\quad \left. + \frac{a\sqrt{\pi}}{n} + a i \pi e^{-n^2} \text{erfc}(-in) \right] e^{ik_0 d_2}, \end{aligned}$$

which can be rewritten in the form

$$\langle G(\mathbf{r}, \mathbf{r}_0) \rangle_R = \left[\frac{1}{4i} R_{\text{eff}}(\kappa_s) \sqrt{\frac{2}{\pi}} \frac{1}{\sqrt{ik_0 d_2}} + \frac{a\sqrt{\pi}}{n} B(n) \right] e^{ik_0 d_2}, \quad (28)$$

where $B(n) = 1 + in\sqrt{\pi} \exp(-n^2) \text{erfc}(-in)$ is the boundary loss factor.

In grazing incidence ($\theta \ll 1$) and for a mean admittance representing a hard ground ($|\langle \beta \rangle| \ll 1$), the expression of the reflected wave can be simplified and be written as a Weyl–Van der Pol formula²⁷

$$\langle G(\mathbf{r}, \mathbf{r}_0) \rangle_R = \frac{1}{4i} \sqrt{\frac{2}{\pi}} \frac{e^{ik_0 d_2}}{\sqrt{ik_0 d_2}} (R_{\text{eff}}(\kappa_s) + [1 - R_{\text{eff}}(\kappa_s)] B(n)), \quad (29)$$

in which the numerical distance is approximated by

$$n = \sqrt{\frac{ik_0 d_2}{2}} [\sin \theta + \beta_{\text{eff}}(\kappa_s)]. \quad (30)$$

Details on the derivation of Eq. (29) are given in [Appendix C](#).

D. Effective admittance and reflection coefficient

The modification of the reflection coefficient due to the random admittance fluctuations is now exemplified. The average surface admittance is that of a hard-backed porous layer of thickness e ,

$$\langle \beta \rangle = \beta_c \tanh(-ik_c e). \quad (31)$$

The characteristic admittance β_c and the propagation constant k_c of the porous layer are prescribed using the Hamet and Bérengrier model²⁹

$$\beta_c = \frac{\Omega}{q} \sqrt{\frac{-i\omega(\omega_3 - i\omega)}{(\omega_1 - i\omega)(\omega_2 - i\omega)}}, \quad (32)$$

$$k_c = \frac{\omega q}{c_0} \sqrt{\frac{(\omega_1 - i\omega)(\omega_3 - i\omega)}{-i\omega(\omega_2 - i\omega)}},$$

where the angular frequencies ω_1 , ω_2 , and ω_3 depend on the ground characteristics through $\omega_1 = \sigma_0 \Omega / (\rho_0 q^2)$, $\omega_2 = \sigma_0 / (\rho_0 \text{Pr})$ and $\omega_3 = \gamma \sigma_0 / (\rho_0 \text{Pr})$. The air density ρ_0 is 1.21 kg m^{-3} and the ratio of specific heats γ is 1.4. The Prandtl number Pr is equal to 0.7. The Hamet and Bérengrier model is preferred to semi-empirical one-parameter models, as it is physically admissible.^{10,28} However, in order to imitate one-parameter models and not to introduce additional parameters, the porosity Ω and tortuosity q are set to 1. We consider two types of ground, which usually represent grassy grounds: in the first one, the air flow resistivity σ_0 is 100 kPa s m^{-2} and $e = \infty$, corresponding to a semi-infinite ground, and in the second one, $\sigma_0 = 100 \text{ kPa s m}^{-2}$ and $e = 0.01 \text{ m}$.

The spectrum of the admittance spatial fluctuations must be specified. However, such spectrum is not available yet from the literature due to the lack of studies reporting measurements of the spatial variations of the acoustic ground

properties. For the sake of simplicity, one considers a Gaussian correlation function

$$\langle \beta'(x) \beta'(x+r) \rangle = \sigma_\beta^2 \exp\left(-\frac{r^2}{L^2}\right), \quad (33)$$

where L is the admittance correlation length. From Eq. (14), the spectrum of the admittance fluctuations is therefore given by

$$W(\kappa) = \sqrt{\pi} L \sigma_\beta^2 \exp\left(-\frac{\kappa^2 L^2}{4}\right) \quad (34)$$

and the effective admittance is obtained with

$$\beta_{\text{eff}}(\kappa) = \langle \beta \rangle - \sigma_\beta^2 \frac{k_0 L}{2\sqrt{\pi}} \int_{-\infty}^{\infty} \frac{\exp\left[-(\kappa - \kappa')^2 L^2 / 4\right]}{\alpha(\kappa') + k_0 \langle \beta \rangle} d\kappa'. \quad (35)$$

Figure 4(a) shows the variation of the effective admittance $\beta_{\text{eff}}[k_0 \cos \theta]$ for grazing angles between 0 and $\pi/2$ and for three stds of the admittance fluctuations. The mean admittance is $0.0116 - 0.1154i$, corresponding to that for the hard backed porous layer with $\sigma_0 = 100 \text{ kPa s m}^{-2}$ and $e = 0.01 \text{ m}$ for $f = 450 \text{ Hz}$. The correlation length is set to $L = 5 \text{ m}$. It is observed that as the grazing angle approaches zero, the real part of the effective admittance increases while the imaginary part is almost constant. In addition, for the same grazing angle, increasing $|\sigma_\beta|$ leads to an increase in $\text{Re}(\beta_{\text{eff}})$. The corresponding effective reflection coefficients $R_{\text{eff}}[k_0 \cos \theta]$ are represented in the complex plane in Fig. 4(b). For a given grazing angle, the amplitude of the reflection coefficient decreases with $|\sigma_\beta|$. This implies that, for the mean pressure, the ground surface becomes more and more absorbing, as the std of the admittance fluctuations increases.

In Fig. 5(a), the variations of the effective impedance are represented for three different correlation lengths. Interestingly, the value of the effective admittance for $\theta = \pi/2$, corresponding to normal incidence is almost independent of the correlation length. For grazing angles close to zero, the real part of the admittance increases with the correlation length and its imaginary part is almost constant. As observed previously, this leads to a decrease in the amplitude of the reflection coefficient in Fig. 5(b). The amplitude of the coherent reflected wave will therefore be reduced as the distance increases and as the correction length or the standard deviation of the admittance increases. This behavior is usually observed in multiple scattering problems for which the coherent field decreases with the distance, the correlation length, and the standard deviation of the fluctuating parameter. This is for instance the case for propagation through an isotropic homogeneous random medium.⁴

E. Surface wave pole

The influence of the admittance randomness on the surface wave component is now investigated. The relation $D(\kappa_p) = 0$ in Eq. (21) relates the horizontal and vertical wavenumbers of the surface waves. It can be solved

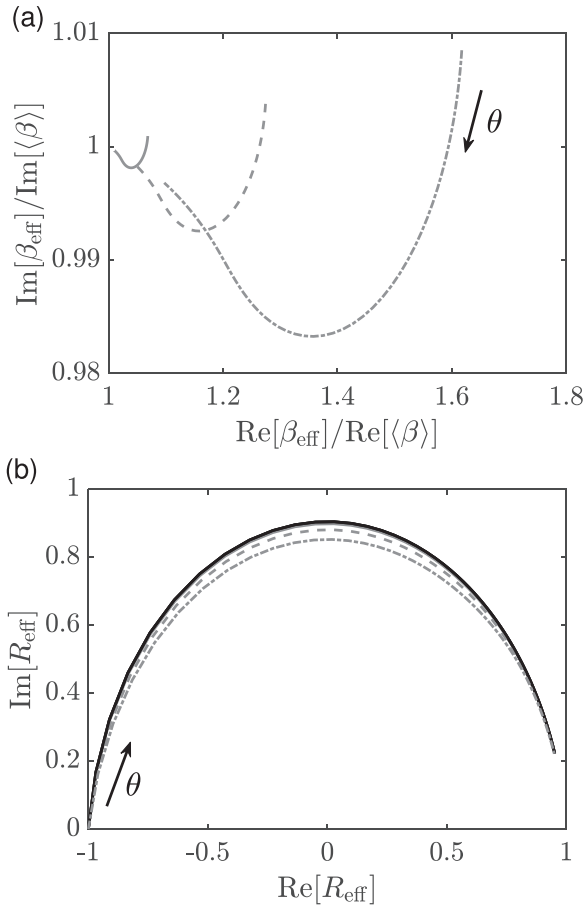


FIG. 4. (a) Effective admittance and (b) corresponding reflection coefficient in the complex plane for grazing angles θ between 0 and $\pi/2$ for $L=5$ m, $f=450$ Hz, and several stds of the admittance fluctuations: (solid gray) $\sigma_\beta = 0.1\langle\beta\rangle$, (dash gray) $\sigma_\beta = 0.2\langle\beta\rangle$ and (dashed-dotted gray) $\sigma_\beta = 0.3\langle\beta\rangle$. The black solid line in (b) corresponds to the reflection coefficient for the average admittance $\langle\beta\rangle = 0.0116 - 0.1154i$.

numerically using the Newton–Raphson algorithm, using as the initial guess the solution of $D(\kappa_p) = 0$ for $\sigma_\beta = 0$, which has been denoted by κ_p^0 in Sec. II C.

If additionally k_0L and $|\sigma_\beta|$ are small compared to one, the effective admittance is close to the average admittance. One can then obtain the pole of the reflection coefficient with the equations

$$\begin{aligned}\kappa_p &= k_0\sqrt{1 - \beta_{\text{eff}}^2(\kappa_p^0)}, \\ \alpha_p &= -k_0\beta_{\text{eff}}(\kappa_p^0).\end{aligned}\quad (36)$$

An example of the variation of the surface wave pole location in the complex plane as the std of the admittance fluctuations $|\sigma_\beta|$ increases is shown in Fig. 6 for three values of L . The mean admittance and the frequency are the same as in Figs. 4 and 5. Typically, for small values of k_0L , the imaginary part of the vertical and horizontal wavenumbers of the surface wave increases with $|\sigma_\beta|$. As for the reflected wave, the amplitude of the coherent surface wave will tend to be smaller than that for a ground with a homogeneous admittance $\langle\beta\rangle$. It is seen also that up to $L=5$ m the approximate solution obtained with Eq. (36) is close to the exact one, obtained by solving $D(\kappa_p) = 0$. For $L=10$ m, deviations

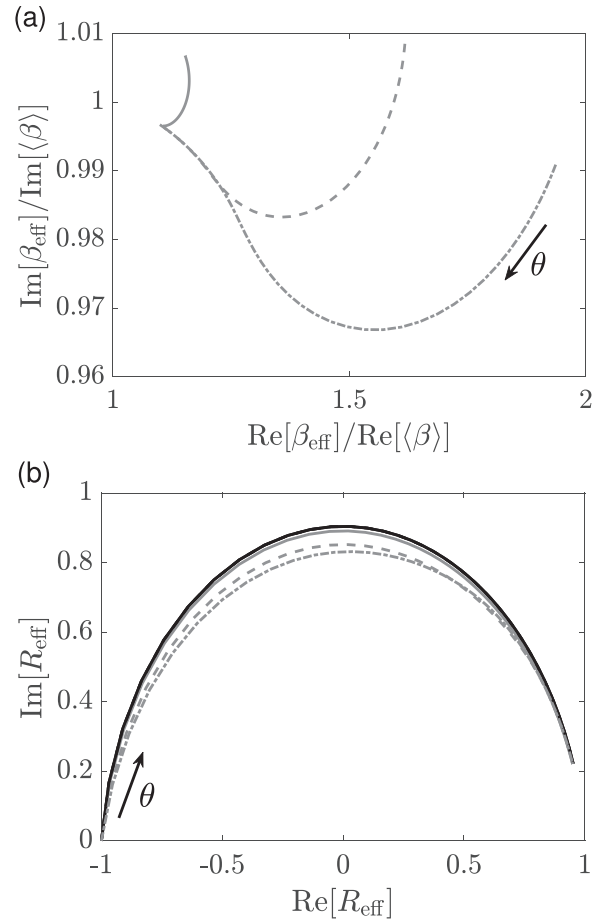


FIG. 5. (a) Effective admittance and (b) corresponding reflection coefficient in the complex plane for grazing angles θ between 0 and $\pi/2$ for $\sigma_\beta = 0.3\langle\beta\rangle$, $f=450$ Hz and several correlation lengths: (solid gray) $L=0.5$ m, (dash gray) $L=5$ m and (dashed-dotted gray) $L=10$ m. The black solid line in (b) corresponds to the reflection coefficient for the average admittance $\langle\beta\rangle = 0.0116 - 0.1154i$.

are however observed. In particular, the imaginary part of α_p is overestimated, which implies that the decrease of the surface wave component with height would be amplified using Eq. (36).

III. NUMERICAL STUDY

A. Numerical specification

Numerical simulations are now performed to study the acoustic field above the ground with a random spatially-varying admittance. The objectives are to compare and validate the analytical expression for the coherent field obtained in Sec. II C and to investigate the variability of the SPLs due to the admittance randomness.

The numerical simulations are carried out using a solver of the two-dimensional linearized Euler equations,³⁰ based on finite-difference time-domain techniques.³¹ The source is located at $(x_0=0, z_0=1)$ m. The domain $[-5\text{ m}; 205\text{ m}] \times [0; 20\text{ m}]$ is discretized using a uniform spatial step $\Delta x = \Delta z = 0.05$ m in the x - and z -directions. The time step Δt is chosen so that the Courant–Friedrichs–Lewy number defined by $\text{CFL} = c_0\Delta t/\Delta x$ is equal to 0.25. A total of 19 200 time iterations are computed. Concerning the parameters of

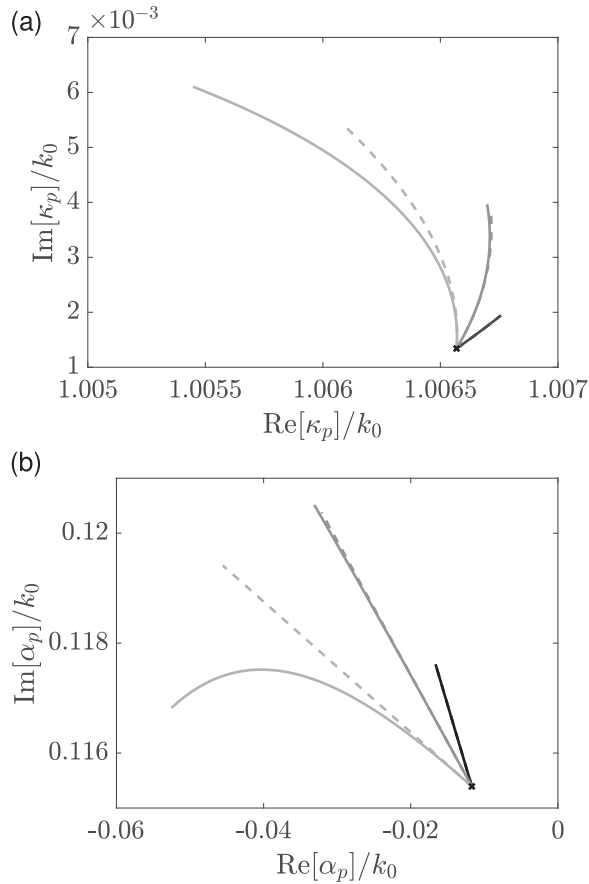


FIG. 6. Variation of the (a) horizontal and (b) vertical wavenumbers of the surface wave as the normalized std of the admittance fluctuations $\sigma_\beta/\langle\beta\rangle$ increases from 0 to 0.5 for a Gaussian spectrum and for: (black) $L=0.5$ m, (dark gray) $L=5$ m and (light gray) $L=10$ m. The mean admittance is $\langle\beta\rangle = 0.0116 - 0.1154i$ and $f=450$ Hz. The solid and dashed lines correspond, respectively, to the numerical solution of the equation $D(\kappa_p)=0$ and to the approximate solution in Eq. (36).

the admittance fluctuations, there is currently no available data in the literature. From the measurements reported in Ref. 11, the normalized std of the admittance fluctuations $|\sigma_\beta/\langle\beta\rangle|$ are between 0.1 and 0.4 for natural grounds and characteristic length scales of variations seem to be in the order of 1 to 10 m. Therefore, we choose correlation lengths of $L=0.5$, 1, and 5 m and a standard deviation $\sigma_\beta = 0.3\langle\beta\rangle$. The admittance spectrum is Gaussian [see Eq. (34)]. For each configuration, 200 realizations of the spatially-varying admittance $\beta(x)$ are performed. In details, the surface admittance is prescribed with $\beta(x) = \langle\beta\rangle(1 + 0.3\epsilon(x))$, where $\epsilon(x)$ is a Gaussian random function of zero mean and unit std and with the desired correlation length. Convergence tests have been done, showing that with this number of realizations, the mean value and the standard deviation of the acoustic pressure and intensity are correctly estimated. High-order moments or even the probability density functions, as obtained by Ehrhardt *et al.*³² for plane wave propagation through a turbulent medium, are not investigated as it would require to have a much higher number of realizations. Finally, the implementation of the time-domain admittance boundary condition is based on a generalized recursive convolution method, described in Troian *et al.*³³

Numerical simulations have been performed for the two ground types presented in Sec. IID. For the parameters of the admittance fluctuations chosen here, the randomness has only a small influence for the semi-infinite ground: typically, the SPL for a particular realization deviates from the unperturbed SPL by at maximum 2 dB over the frequency bandwidth of interest. Results obtained for the hard-backed porous layer of flow resistivity $\sigma = 100 \text{ kPa s m}^{-2}$ and of thickness $e = 0.01$ m are more noticeable and are considered hereafter.

B. Acoustic mean pressure

Figure 7 shows the average pressure relative to the free-field, along with the unperturbed pressure obtained for a ground with a homogeneous admittance $\langle\beta\rangle$ as a function of the frequency for receivers at a distance $x=200$ m and at heights $z=2$ and 5 m. For both source-receiver geometries, the influence of admittance randomness is only significant for frequencies between 300 and 600 Hz. At low and high frequencies, the average pressure is thus close to the unperturbed pressure. A noticeable effect of admittance randomness is to shift the first ground dip toward lower frequencies, as if the ground was more absorbing. Thus, the first ground dip is located at a frequency of 500 Hz for the unperturbed

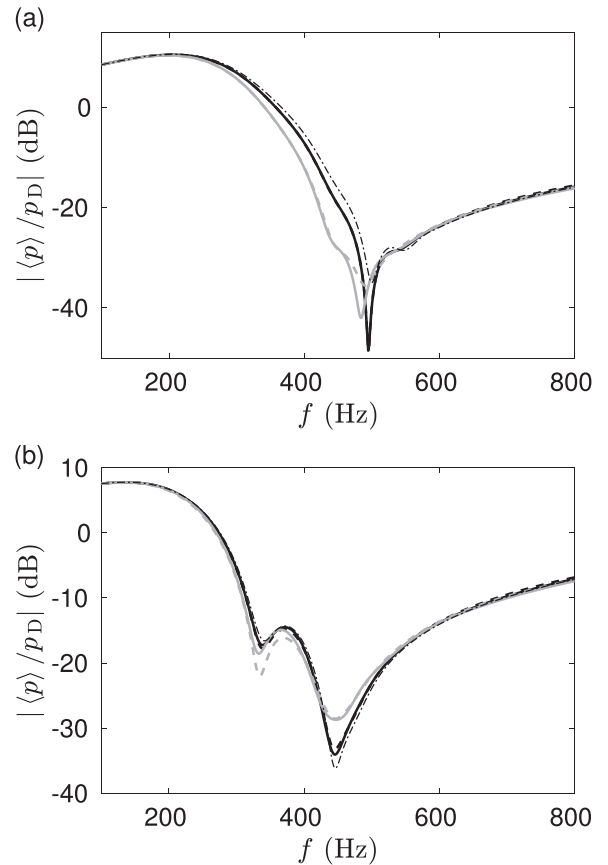


FIG. 7. Sound pressure relative to the free field as a function of the frequency for a receiver located at $x=200$ m and (a) $z=2$ m and (b) $z=5$ m: (thin dashed-dotted) unperturbed pressure obtained for a homogeneous ground of admittance $\langle\beta\rangle$ and average pressure computed (thick solid) from the numerical simulations by an ensemble-averaging over 200 realizations and (dashed) from the analytical solution under the Bourret approximation [Eq. (28)]: (black) $L=0.5$ m and (gray) $L=5$ m.

problem, but in the random case it is at 495 Hz for $L = 0.5$ m and 490 Hz for $L = 5$ m. This effect was also noticed for random roughness.²² Besides, the agreement between the mean pressure computed with the Bouret approximation and by an ensemble-averaging over 200 realizations is satisfactory. In particular, for $L = 0.5$ m, the curves depicting these two solutions are almost superimposed for both receiver heights. For $L = 5$ m, some discrepancies can be observed for frequencies corresponding to the spectrum minima. Indeed, the SPL near destructive interferences is very sensitive to the admittance, and the number of realizations in the averaging process might be insufficient to correctly compute the mean pressure in this particular frequency range.

The variations of the mean pressure with range are shown in Fig. 8 for a line of receivers at a height $z = 2$ m and for two frequencies. Results for $f = 400$ Hz in Fig. 8(a) exemplify the typical variations of the mean pressure. Indeed, it decreases more rapidly with range than the unperturbed pressure due to the loss of coherence of the reflected wave. In addition, greater the correlation length, more rapid the decrease with the distance. This is in accordance with Sec. IID, in which it was observed that the amplitude of the effective reflection coefficient for the random admittance is smaller than that for the mean admittance and that it

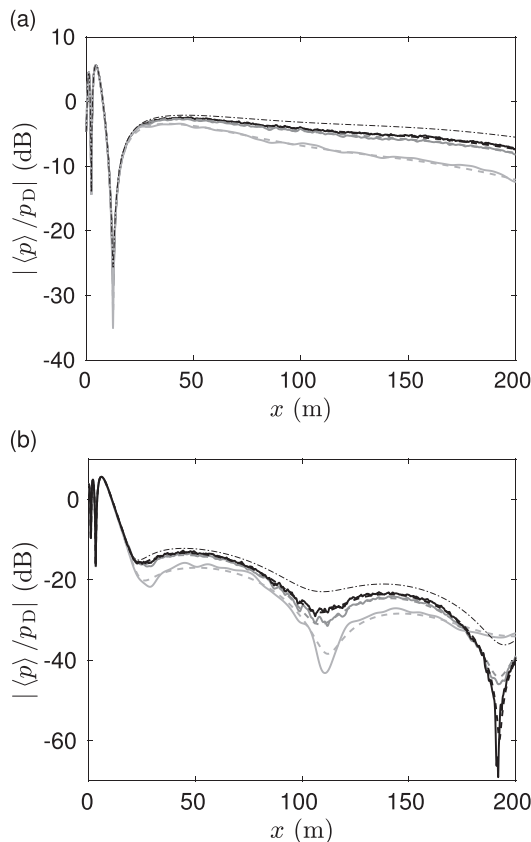


FIG. 8. Sound pressure relative to the free field as a function of the distance for (a) $f = 400$ Hz and (b) $f = 500$ Hz for a line of receivers whose height is $z = 2$ m: (thin dashed-dotted) unperturbed pressure obtained for a homogeneous ground of admittance $\langle\beta\rangle$ and average pressure computed (thick solid) from the numerical simulations by an ensemble-averaging over 200 realizations and (dashed) from the analytical solution under the Bouret approximation [Eq. (28)]: (black) $L = 0.5$ m, (dark gray) $L = 1$ m and (light gray) $L = 5$ m.

decreases with the increase of the correlation length. For $f = 500$ Hz, similar trends are observed. A particular behavior is observed close to the destructive interference pattern at $x = 190$ m. While the interference dip is enhanced for $L = 0.5$ and 1 m, it is reduced for the largest correlation length, i.e., $L = 5$ m, implying that the amplitude of the mean pressure for the random case is larger than that for the deterministic case. Indeed, due to randomness, the phase and amplitude of the reflected wave is modified, and the direct and reflected waves do not cancel each other anymore. In addition, as noticed previously for the spectra in Fig. 7, the mean pressure computed by an ensemble-averaging over 200 realizations and with the Bouret approximation are in close agreement for all cases shown in Fig. 8. Finally, although not plotted in Figs. 7 and 8, the Weyl–Van der Pol formula in Eq. (29) yields similar results than the asymptotic expression in Eq. (28): the largest deviation from the predicted SPL is only about 0.1 dB.

C. Mean intensity and variability

Figure 9 depicts the variations of the sound intensity $I = pp^*$ with the frequency at two receivers at $x = 200$ m and at $z = 2$ and 5 m, already considered in Fig. 7, for the 200 realizations of the admittance and for the correlation length $L = 0.5$ m. In accordance with the fact that the coherent pressure is close to the unperturbed pressure, it is observed that

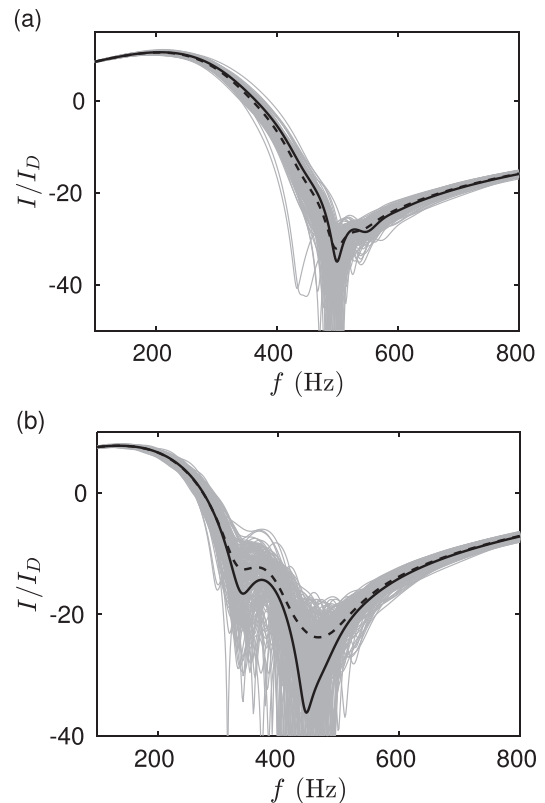


FIG. 9. Intensity relative to the free field as a function of the frequency for a receiver located at $x = 200$ m and (a) $z = 2$ m and (b) $z = 5$ m: (black solid) unperturbed intensity obtained for a homogeneous ground of admittance $\langle\beta\rangle$, (gray solid) intensity obtained for the 200 realizations of the admittance and (black dashed) mean intensity. The correlation length of the admittance fluctuations is $L = 0.5$ m.

the variability for frequencies below 300 Hz and above 600 Hz is quite small for both source-receiver geometries. The intensity for a particular realization of the admittance may deviate from the mean value by at most 3 dB. In the interference region between 300 and 600 Hz, the variability is large, especially at the first ground dip, for which the deviation in the SPL from the mean value can reach 30 dB. In addition, it is observed that at $z=2$ m, the mean intensity is very close to the unperturbed intensity. For $z=5$ m, the same behavior is seen, except for frequencies between 300 and 600 Hz, for which the interference minima obtained for the unperturbed intensity are filled. This effect is largely known in the literature for sound propagation through turbulence near a reflective surface.^{4,34,35} The close correspondence between the mean intensity and the intensity computed in the non-random case has already been noticed by Ostashev *et al.*¹⁴ for the case of a homogeneous random absorbing plane. The corresponding normalized standard deviations of

intensity fluctuations $\sigma_I/\langle I \rangle$, with $\sigma_I = \sqrt{\langle (I - \langle I \rangle)^2 \rangle}$, are shown in Fig. 10 for the receiver height $z=2$ m and for the three correlation lengths. In accordance with Fig. 9(a), it is small at low and high frequencies and has a peak for $f=500$ Hz corresponding to the ground dip. As the correlation length increases, the std of intensity fluctuations increases over the whole spectrum.

Figure 11 shows the variation of the intensity with the distance for a line of receivers at a height $z=2$ m and for the 200 realizations of the admittance. The correlation length is $L=0.5$ m and the frequency is 400 Hz. In the near field, the intensity obtained for all realizations is similar. Variability increases with distance and is particularly high at the interference minima, here at $x=15$ m. In addition, as observed in Fig. 9, the mean intensity is close to the unperturbed intensity for all distances. The normalized standard deviation of the intensity fluctuations at the same line of receivers and for the same frequency is depicted in Fig. 12. Following the previous comments, it presents two peaks at the two interference minima. For $x > 30$ m, it reaches a plateau for $L=0.5$, 1, and 5 m, but increases with the distance starting from $x=160$ m for $L=5$ m. As observed in Fig. 10, the increase of the correlation length leads to an increase of the standard

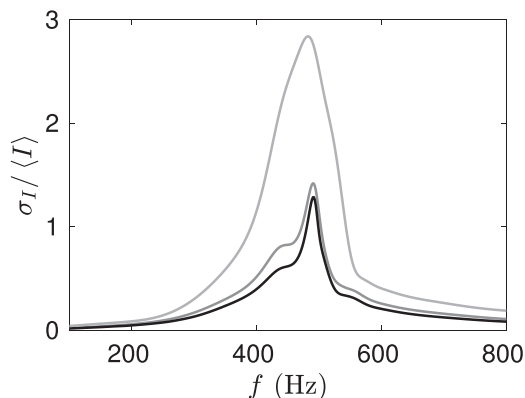


FIG. 10. Normalized standard deviation of intensity fluctuations as a function of the frequency for a receiver located at $x=200$ m and $z=2$ m and for three correlation lengths: (black) $L=0.5$ m, (dark gray) $L=1$ m, and (light gray) $L=5$ m.

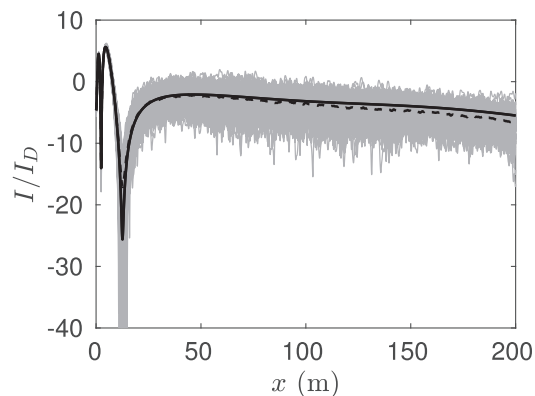


FIG. 11. Intensity relative to the free field as a function of the distance for $f=400$ Hz for a line of receivers whose height is $z=2$ m: (black solid) unperturbed intensity obtained for a homogeneous ground of admittance, (gray solid) intensity obtained for the 200 realizations of the admittance, and (black dashed) mean intensity.

deviation of the intensity fluctuations. In addition, $\sigma_I/\langle I \rangle$ is also plotted in Fig. 12 for a ground with a homogeneous but random admittance, corresponding to an infinite correlation length. It has been computed using the analytical solution for the propagation above a ground with a homogeneous admittance and by considering the admittance as a random variable whose normalized fluctuations $\beta'/\langle \beta \rangle$ follow a normal distribution with a zero mean value and a standard deviation equal to 0.3. It is observed that the std of the intensity fluctuations is maximum in this case. As noticed in Ref. 14, it monotonically increases with the distance at long range, meaning that for a particular realization of the admittance, the intensity is expected to deviate more and more from the mean intensity as the range increases.

IV. CONCLUSION

This study aimed at estimating the influence of the spatial variations of the ground surface admittance on the acoustic field, in the context of outdoor sound propagation. For this purpose, the spatially-varying admittance was treated as a random variable. Starting from an integral equation obtained with the Green's theorem, the Dyson equation for the coherent Green's function was formulated. Using the

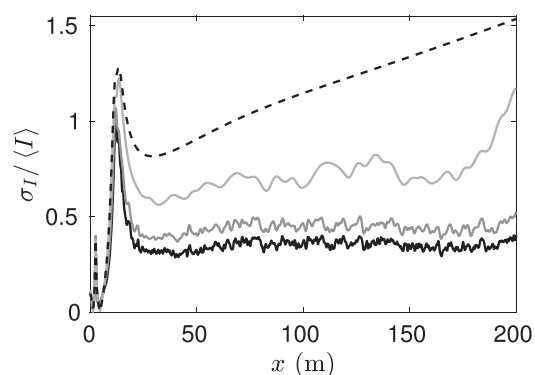


FIG. 12. Normalized standard deviation of intensity fluctuations as a function of the distance for $f=400$ Hz and for four correlation lengths: (black solid) $L=0.5$ m, (dark gray solid) $L=1$ m, (light gray solid) $L=5$ m, and (black dashed) $L=\infty$.

Bourret approximation, an explicit expression was obtained, which extends previous results obtained in the literature.^{15,16} The range of applicability of the Bourret approximation was investigated. The coherent Green's function was then recast in a similar form as the Green's function for a ground with a homogeneous admittance, with an effective admittance that depends on the correlation function of the random admittance fluctuations. An asymptotic expression was obtained at long range and it was exemplified that the randomness tends to reduce the amplitude of the reflection coefficient.

Numerical simulations were then performed using a solver of the linearized Euler equations for two ground types. Ensemble-averaged pressure field over 200 realizations of the spatially-varying admittance was in close agreement with the analytical solution under the Bourret approximation. In addition, the mean intensity does not differ much from the intensity for the nonrandom case, except near destructive interferences. Intensity fluctuations were then investigated. For the considered examples, they were negligible for the semi-infinite ground but were noticeable for the hard-backed porous layer. In particular, the intensity for a specific realization of the spatially-varying admittance can be significantly different from the mean value for the latter case. Finally, the standard deviation of intensity fluctuations obtained for a ground with a random spatially-varying admittance was found to be smaller than that for a random homogeneous admittance plane.

There are several ways to pursue this work. First, this study was limited to a 2D configuration. While we do not expect the underlying physics to be much different, it would be worthwhile to investigate the three-dimensional equivalent problem. There is also a need to have further experimental studies, reporting space and time variations of the surface admittance or corresponding acoustical parameters of natural grounds. It would be interesting to have a database reporting, for outdoor surfaces, along with typical values of the parameters of impedance model, standard deviations and characteristic length scales of variations, as partly done by Martens *et al.*³⁶ and Guillaume *et al.*¹¹ It could be used to quantify the uncertainty in the SPL prediction related to the ground properties. Besides, physical insight can still be gained from analytical studies. In particular, the two-point correlation function of the acoustic pressure can be obtained through the Bethe–Salpether equation, which can be solved under approximations similar to those employed in this paper. The mean intensity and the scattering cross section could thus be examined. In addition, numerical simulations could be used to study higher order moments, such as the standard deviation of the intensity fluctuations, that cannot be obtained in closed forms analytically.

ACKNOWLEDGMENTS

This work was supported by the LabEx Centre Lyonnais d'Acoustique of Université de Lyon, operated by the French National Research Agency (ANR-10-LABX-0060/ANR-11-IDEX-0007). It was granted access to the HPC resources of IDRIS under the allocation 2016-82203 made by GENCI.

APPENDIX A: DERIVATION OF THE EFFECTIVE ADMITTANCE

Details on the derivation of the effective admittance in Sec. II B are given in this appendix. Starting from Eq. (9), the Fourier transform of the average Green's function is split into

$$\langle \hat{G}(\kappa, z, z_0) \rangle = \hat{G}_0(\kappa, z, z_0) + \langle \hat{G}'(\kappa, z, z_0) \rangle, \quad (\text{A1})$$

where \hat{G}_0 is the Fourier transform of the Green's function for the unperturbed problem and $\langle \hat{G}' \rangle$ is the sound pressure perturbation induced by the admittance randomness given by the integral equation

$$\begin{aligned} \langle \hat{G}'(\kappa, z, z_0) \rangle &= -k_0^2 \hat{G}_0(\kappa, z, z_1) \int_{-\infty}^{\infty} e^{-i\kappa(x_1-x_0)} \\ &\quad \times \langle \beta'(x_1)\beta'(x_2) \rangle G_0(\mathbf{r}_1, \mathbf{r}_2) \\ &\quad \times \langle G(\mathbf{r}_2, \mathbf{r}_0) \rangle dx_1 dx_2. \end{aligned}$$

Introducing the Fourier transform of the correlation function W given in Eq. (14) leads to

$$\begin{aligned} \langle \hat{G}'(\kappa, z, z_0) \rangle &= -\frac{k_0^2}{2\pi} \hat{G}_0(\kappa, z, z_1) \int_{-\infty}^{\infty} e^{-i\kappa(x_1-x_0)} \\ &\quad \times \int_{-\infty}^{\infty} W(\kappa') e^{-i\kappa'(x_2-x_1)} d\kappa' G_0(\mathbf{r}_1, \mathbf{r}_2) \\ &\quad \times \langle G(\mathbf{r}_2, \mathbf{r}_0) \rangle dx_1 dx_2, \end{aligned}$$

which can be rewritten as

$$\begin{aligned} \langle \hat{G}'(\kappa, z, z_0) \rangle &= -\frac{k_0^2}{2\pi} \hat{G}_0(\kappa, z, z_1) e^{i\kappa x_0} \int_{-\infty}^{\infty} W(\kappa') \\ &\quad \times \int_{-\infty}^{\infty} G_0(\mathbf{r}_1, \mathbf{r}_2) e^{-i(\kappa-\kappa')x_1} dx_1 \\ &\quad \times \langle G(\mathbf{r}_2, \mathbf{r}_0) \rangle e^{-i\kappa'x_2} d\kappa' dx_2. \end{aligned}$$

Taking the Fourier transform along the x_1 -direction in the preceding equation yields

$$\begin{aligned} \langle \hat{G}'(\kappa, z, z_0) \rangle &= -\frac{k_0^2}{2\pi} \hat{G}_0(\kappa, z, z_1) \\ &\quad \times \int_{-\infty}^{\infty} W(\kappa') \hat{G}_0(\kappa - \kappa', z_1, z_2) \\ &\quad \times \int_{-\infty}^{\infty} \langle G(\mathbf{r}_2, \mathbf{r}_0) \rangle e^{-i\kappa(x_2-x_0)} dx_2 d\kappa', \end{aligned}$$

which after a Fourier transform along the x_2 -direction gives

$$\begin{aligned} \langle \hat{G}'(\kappa, z, z_0) \rangle &= -\frac{k_0^2}{2\pi} \hat{G}_0(\kappa, z, z_1) \langle \hat{G}(\kappa, z_2, z_0) \rangle \\ &\quad \times \int_{-\infty}^{\infty} W(\kappa') \hat{G}_0(\kappa - \kappa', z_1, z_2) d\kappa'. \quad (\text{A2}) \end{aligned}$$

Combining Eqs. (A1) and (A2) leads to Eq. (11).

APPENDIX B: RANGE OF APPLICABILITY OF THE BOURRET APPROXIMATION

Necessary conditions for the applicability of the Bourret approximation are derived. For this purpose, following Rytov *et al.*,²⁰ we consider the next approximation of the mass operator, which appears in the Dyson equation in Eq. (7),

$$M(\mathbf{r}_1, \mathbf{r}_2) \approx \left\langle V(x_1) \langle G \rangle^{(1)}(\mathbf{r}_1, \mathbf{r}_2) V(x_2) \right\rangle \\ = -k_0^2 \langle \beta'(x_1) \beta'(x_2) \rangle \langle G \rangle^{(1)}(\mathbf{r}_1, \mathbf{r}_2),$$

where $\langle G \rangle^{(1)}$ is the average Green's function in the Bourret approximation. The diagrammatic form of the Dyson equation with this approximation is depicted in Fig. 2. Using the procedure detailed in Sec. II B, the average Green's function can also be determined in this approximation. The effective admittance is now written as

$$\beta_{\text{eff}}^{(2)}(\kappa) = \langle \beta \rangle - \frac{k_0}{2\pi} \int_{-\infty}^{\infty} \frac{W(\kappa - \kappa')}{\alpha(\kappa') + k_0 \beta_{\text{eff}}^{(1)}(\kappa')} d\kappa', \quad (\text{B1})$$

where $\beta_{\text{eff}}^{(1)}$ is the effective admittance in the Bourret approximation, given in Eq. (17). It is therefore required so that the Bourret approximation is valid that the modulus of the correction $|\beta_{\text{eff}}^{(2)}(\kappa) - \beta_{\text{eff}}^{(1)}(\kappa)|$ is small compared to the difference between the effective admittance and the mean admittance, which yields

$$|\beta_{\text{eff}}^{(2)}(\kappa) - \beta_{\text{eff}}^{(1)}(\kappa)| \ll |\beta_{\text{eff}}^{(1)}(\kappa) - \langle \beta \rangle|. \quad (\text{B2})$$

The correction $\beta_{\text{eff}}^{(2)}(\kappa) - \beta_{\text{eff}}^{(1)}(\kappa)$ can be explicitly written as

$$\beta_{\text{eff}}^{(2)}(\kappa) - \beta_{\text{eff}}^{(1)}(\kappa) \\ = \frac{k_0^2}{2\pi} \int_{-\infty}^{\infty} W(\kappa - \kappa') \\ \times \frac{\beta_{\text{eff}}^{(1)}(\kappa') - \langle \beta \rangle}{(\alpha(\kappa') + k_0 \langle \beta \rangle) (\alpha(\kappa') + k_0 \beta_{\text{eff}}^{(1)}(\kappa'))} d\kappa'.$$

At the first order, we can approximate $\beta_{\text{eff}}^{(1)}(\kappa') \approx \langle \beta \rangle$ in the denominator of the integrand to get

$$\beta_{\text{eff}}^{(2)}(\kappa) - \beta_{\text{eff}}^{(1)}(\kappa) = \frac{k_0^2}{2\pi} \int_{-\infty}^{\infty} W(\kappa - \kappa') \\ \times \frac{\beta_{\text{eff}}^{(1)}(\kappa') - \langle \beta \rangle}{(\alpha(\kappa') + k_0 \langle \beta \rangle)^2} d\kappa'. \quad (\text{B3})$$

The condition in Eq. (B2) must be *a priori* verified for all wavenumbers because the reflected wave in the physical space in Eq. (20) is obtained by integration over the real κ -axis. However, due to the term e^{iz} , the contributions for $\kappa/k_0 \gg 1$ are negligible and the condition in Eq. (B2) can be checked for small and moderate values of κ/k_0 .

For $k_0 L \gg 1$, as indicated in Appendix D, the correlation function can be approximated by $W(\kappa) \approx 2\pi\sigma_\beta^2 \delta(\kappa)$. The integrals appearing in Eqs. (17) and (B3) can be evaluated, and Eq. (B2) reduces to

$$\frac{k_0^2 |\sigma_\beta|^2}{|\alpha(\kappa) + k_0 \langle \beta \rangle|^2} \ll 1.$$

It can be shown that the minimum of $|\alpha(\kappa) + k_0 \langle \beta \rangle|$ over the real axis is obtained at $\kappa = k_0 \sqrt{1 + \text{Im}[\langle \beta \rangle]^2}$ and is equal to $k_0 \text{Re}[\langle \beta \rangle]$ if $\text{Im}[\langle \beta \rangle] \leq 0$ and is obtained at $\kappa = k_0$ and is equal to $k_0 |\langle \beta \rangle|$ if $\text{Im}[\langle \beta \rangle] \geq 0$. Therefore, the condition of applicability of the Bourret approximation is $|\sigma_\beta|^2 / \text{Re}[\langle \beta \rangle]^2 \ll 1$, if $\text{Im}[\langle \beta \rangle] \leq 0$ and $|\sigma_\beta|^2 / |\langle \beta \rangle|^2 \ll 1$, if $\text{Im}[\langle \beta \rangle] \geq 0$.

For $k_0 L \ll 1$, the calculation is more complex, because the integrals in Eqs. (17) and (B3) have no closed-form expressions. We can however get approximate values by assuming that the correlation function $W(\kappa)$ acts as an ideal low-pass filter that eliminates wavenumbers with $|\kappa| > 1/L$, which yields $W(\kappa) = \sigma_\beta^2 L \pi H[1/L - |\kappa|]$. With this assumption and introducing the change of variables $u = \kappa'/k_0$, we obtain

$$\beta_{\text{eff}}^{(1)}(\kappa) - \langle \beta \rangle \approx -\frac{k_0 L \sigma_\beta^2}{2} \int_{-u^-}^{u^+} \frac{1}{\sqrt{1-u^2} + \langle \beta \rangle} du,$$

where the limits of integration are $u^- = (\kappa L - 1)/k_0 L$ and $u^+ = (\kappa L + 1)/k_0 L$. For $\kappa L \ll 1$, we can approximate u^- and u^+ by $-1/k_0 L$ and $1/k_0 L$, so that $\beta_{\text{eff}}^{(1)} - \langle \beta \rangle$ does not depend on κ . In addition, as $k_0 L \ll 1$, the main contributions to the integral are obtained for $|u| \gg 1$, so that we can use the approximation $\sqrt{1-u^2} \approx i|u|$. We therefore get

$$\beta_{\text{eff}}^{(1)}(\kappa) - \langle \beta \rangle \approx -\frac{k_0 L \sigma_\beta^2}{2} \int_{-1/k_0 L}^{1/k_0 L} \frac{1}{i|u| + \langle \beta \rangle} du,$$

which at the leading order in $1/k_0 L$ gives

$$\beta_{\text{eff}}^{(1)}(\kappa) - \langle \beta \rangle \approx -ik_0 L \sigma_\beta^2 \log(k_0 L). \quad (\text{B4})$$

Concerning $\beta_{\text{eff}}^{(2)} - \beta_{\text{eff}}^{(1)}$, one gets similarly

$$\beta_{\text{eff}}^{(2)}(\kappa) - \beta_{\text{eff}}^{(1)}(\kappa) \approx \frac{k_0 L \sigma_\beta^2}{2} \int_{-u^-}^{u^+} \frac{\beta_{\text{eff}}^{(1)}(k_0 u) - \langle \beta \rangle}{(\sqrt{1-u^2} + \langle \beta \rangle)^2} du.$$

As the denominator in the integrand behaves as u^2 for $u \gg 1$, the contributions for $u \gg 1$ are negligible. Therefore, we can approximate $\beta_{\text{eff}}^{(1)}(k_0 u) - \langle \beta \rangle$ using Eq. (B4) and extend the limits of integration to infinity to get

$$\beta_{\text{eff}}^{(2)}(\kappa) - \beta_{\text{eff}}^{(1)}(\kappa) \approx -\frac{ik_0^2 L^2 \sigma_\beta^4}{2} \log(k_0 L) \\ \times \int_{-\infty}^{\infty} \frac{1}{(\sqrt{1-u^2} + \langle \beta \rangle)^2} du. \quad (\text{B5})$$

As usually $|\beta| \ll 1$ for natural grounds, the integral in the preceding equation is approximately equal to its value for $\langle \beta \rangle = 0$, which is $i\pi$. Finally, inserting Eqs. (B4) and (B5) into Eq. (B2) gives the condition of applicability of the Bourret approximation for $k_0 L \ll 1$, which is $|\sigma_\beta|^2 k_0 L \ll 1$.

APPENDIX C: WEYL–VAN DER POL FORMULA

In this appendix, we show that the expression of the reflected wave in Eq. (28) can be expressed as a Weyl–Van der Pol formula in grazing incidence ($\theta \ll 1$), for a mean admittance representing a hard ground ($|\langle\beta\rangle| \ll 1$) and for weak fluctuations ($|\sigma_\beta|^2 \ll 1$ and $k_0L \ll 1$).

Indeed, as $|\sigma_\beta|^2 \ll 1$ and $k_0L \ll 1$, we can use the simplified expressions of the surface wave wavenumbers given in Eq. (36). Moreover, as $|\langle\beta\rangle| \ll 1$, one has $\kappa_p \approx k_0(1 - \beta_{\text{eff}}^2(\kappa_p^0)/2)$. The numerical distance n can therefore be approximated by

$$n \approx \sqrt{ik_0d_2} \left[1 - \left(1 - \frac{\beta_{\text{eff}}^2(\kappa_p^0)}{2} \right) \cos \theta + \beta_{\text{eff}}(\kappa_p^0) \sin \theta \right]^{1/2}.$$

In addition, at the first order in θ and $\langle\beta\rangle$, $\kappa_p^0 = k_0\sqrt{1 - \langle\beta\rangle^2} \approx k_0 \cos \theta$, so that $\beta_{\text{eff}}(\kappa_p^0) \approx \beta_{\text{eff}}(\kappa_s)$ and, similarly, $\beta_{\text{eff}}(\kappa_p) \approx \beta_{\text{eff}}(\kappa_s)$. Approximating $\cos \theta \approx 1 - \theta^2/2$ and $\sin \theta \approx \theta$, at the first order, one has

$$n \approx \sqrt{\frac{ik_0d_2}{2}} (\sin \theta + \beta_{\text{eff}}(\kappa_s)).$$

The parameter a in Eq. (25) can also be simplified. Indeed, at the first order, one has

$$a \approx \frac{k_0\beta_{\text{eff}}(\kappa_s)}{2\pi i\kappa_p} \approx \frac{\beta_{\text{eff}}(\kappa_s)}{2\pi i}.$$

Finally, introducing the approximations of n and a in Eq. (28) leads to the Weyl–Van der Pol formula in Eq. (29).

APPENDIX D: MEAN ACOUSTIC PRESSURE FOR A RANDOM ADMITTANCE HOMOGENEOUS PLANE AND FAR-FIELD ASYMPTOTIC EXPRESSION

In this appendix, one considers a homogeneous absorbing plane with a random admittance $\beta = \langle\beta\rangle + \beta'$, which can also be interpreted as a high-frequency or small-wavelength limit ($k_0L \gg 1$) of the problem considered in Sec. II. As shown in Appendix B, a necessary condition for the validity of the Bourret approximation is that $|\sigma_\beta|^2 \ll \text{Re}[\langle\beta\rangle]^2$, if $\text{Im}[\langle\beta\rangle] \leq 0$ and $|\sigma_\beta|^2 \ll |\langle\beta\rangle|^2$, if $\text{Im}[\langle\beta\rangle] \geq 0$.

In this case, one has $\beta'(x+r)\beta'(x) = \beta'^2$ yielding a correlation function $\langle\beta'(x+r)\beta'(x)\rangle = \sigma_\beta^2$. The admittance spectrum is thus given by $W(\kappa) = 2\pi\sigma_\beta^2\delta(\kappa)$. In the Bourret approximation, the effective admittance is obtained using Eq. (17),

$$\beta_{\text{eff}}(\kappa) = \langle\beta\rangle - \frac{k_0\sigma_\beta^2}{\alpha(\kappa) + k_0\langle\beta\rangle}. \quad (\text{D1})$$

Inserting this relation in Eq. (16), the effective reflection coefficient is thus given by

$$R_{\text{eff}}(\kappa) = \frac{\alpha^2 - k_0^2(\langle\beta\rangle^2 - \sigma_\beta^2)}{(\alpha + k_0\langle\beta\rangle)^2 - k_0^2\sigma_\beta^2},$$

which can be decomposed into

$$R_{\text{eff}}(\kappa) = \frac{1}{2} \left(\frac{\alpha - k_0(\langle\beta\rangle - \sigma_\beta)}{\alpha + k_0(\langle\beta\rangle - \sigma_\beta)} + \frac{\alpha - k_0(\langle\beta\rangle + \sigma_\beta)}{\alpha + k_0(\langle\beta\rangle + \sigma_\beta)} \right). \quad (\text{D2})$$

The effective reflection coefficient is therefore equal to the average of the reflection coefficients obtained for homogeneous grounds of admittances $\langle\beta\rangle + \sigma_\beta$ and $\langle\beta\rangle - \sigma_\beta$. Note also that, for $k_0L \gg 1$, the effective reflection coefficient has two poles, located at $\alpha_p^\pm = -k_0(\langle\beta\rangle \pm \sigma_\beta)$ and $\kappa_p^\pm = k_0\sqrt{1 - (\langle\beta\rangle \pm \sigma_\beta)^2}$.

From Eq. (D2), the reflected wave can thus be written as

$$\langle G(\mathbf{r}, \mathbf{r}_0) \rangle_R = \frac{1}{2} \left[G_0(\mathbf{r}, \mathbf{r}_0, \langle\beta\rangle + \sigma_\beta)_R + G_0(\mathbf{r}, \mathbf{r}_0, \langle\beta\rangle - \sigma_\beta)_R \right], \quad (\text{D3})$$

where

$$G_0(\mathbf{r}, \mathbf{r}_0, \beta)_R = \left[\frac{1}{4i} R_0(\kappa_s) \sqrt{\frac{2}{\pi}} \frac{1}{\sqrt{ik_0d_2}} + \frac{a_0\sqrt{\pi}}{n_0} B(n_0) \right] e^{ik_0d_2}$$

is the reflected wave for sound propagation over a homogeneous ground of admittance β . In this equation, the reflection coefficient is

$$R_0(\kappa_s = k_0 \cos \theta) = \frac{\sin \theta - \beta}{\sin \theta + \beta}.$$

The parameter a_0 and the numerical distance n_0 are given by

$$a_0 = \frac{1}{2\pi i} \frac{\beta}{\sqrt{1 - \beta^2}},$$

$$n_0 = \sqrt{ik_0d_2} \left(1 - \sqrt{1 - \beta^2} \cos \theta + \beta \sin \theta \right)^{1/2}.$$

For grazing incidence and for $|\langle\beta\rangle - \sigma_\beta| \ll 1$ and $|\langle\beta\rangle + \sigma_\beta| \ll 1$, the Weyl–Van der Pol formula can also be employed

$$G_0(\mathbf{r}, \mathbf{r}_0, \beta)_R = \frac{1}{4i} \sqrt{\frac{2}{\pi}} \frac{e^{ik_0d_2}}{\sqrt{ik_0d_2}} \times (R_0(\kappa_s) + [1 - R_0(\kappa_s)]B(n_0)),$$

with the numerical distance approximated by

$$n_0 = \sqrt{\frac{ik_0d_2}{2}} (\sin \theta + \beta).$$

From Eq. (D1), an effective admittance can also be obtained in this case and is given by

$$\beta_{\text{eff}}(k_0 \cos \theta) = \langle\beta\rangle - \frac{\sigma_\beta^2}{\sin \theta + \langle\beta\rangle}. \quad (\text{D4})$$

Note that it can be retrieved in a similar way as done in Sec. IIB of Ref. 14. In addition, the effective admittance is not equal to the inverse of the effective impedance given in Eq. (12) of Ref. 14.

Figure 13 shows the mean pressure for a line of receivers located between $x=0$ and 200 m at a height $z=2$ m and for the two grounds presented in Sec. IID. The source height is 1 m and the frequency is 500 Hz. The admittance fluctuations follow a normal distribution and two standard deviations, which are $\sigma_\beta = 0.25 \operatorname{Re}\{\langle\beta\rangle\}$ and $\sigma_\beta = 0.25\langle\beta\rangle$, are considered. For the semi-infinite ground in Fig. 13(a), as indicated in Sec. III A, the mean pressure is very close to the unperturbed pressure in both cases. Deviations from the unperturbed pressure are more noticeable for the hard backed porous layer in Fig. 13(b). For the std of $\sigma_\beta = 0.25 \operatorname{Re}\{\langle\beta\rangle\}$, the mean pressure obtained in the Bourret approximation is close to that computed by ensemble averaging over 1000 realizations. On the contrary, for the std $\sigma_\beta = 0.25\langle\beta\rangle$, a large error is obtained with the Bourret approximation starting from $x=40$ m. This behavior can be explained as because $\langle\beta\rangle = 0.0144 - 0.128i$, the necessary condition for applying the Bourret approximation $|\sigma_\beta|^2 \ll \operatorname{Re}\{\langle\beta\rangle\}^2$ is not satisfied in this case.

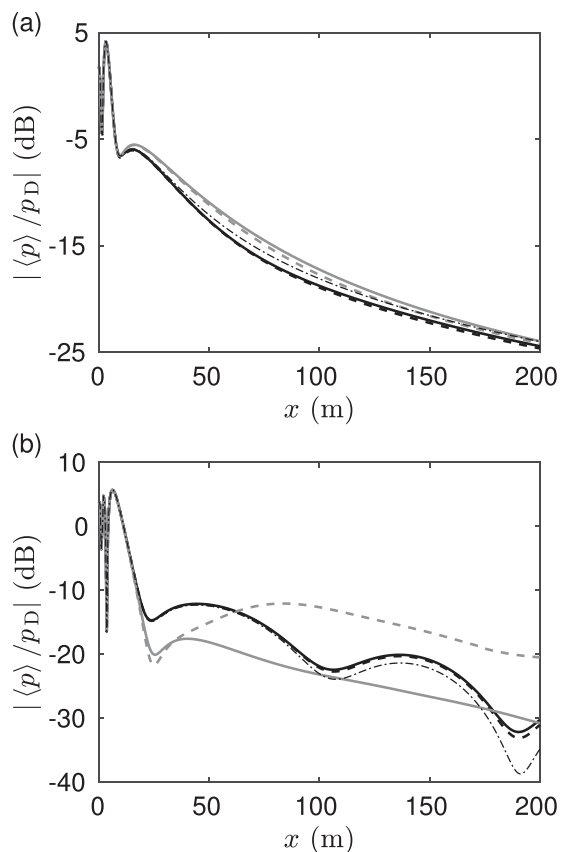


FIG. 13. Sound level relative to the free field as a function of the distance (a) for a semi-infinite ground and $f=300$ Hz and (b) for a hard backed porous layer and $f=500$ Hz: (thin dashed-dotted) unperturbed pressure obtained for a homogeneous ground of admittance $\langle\beta\rangle$ and average pressure computed (solid) over 1000 realizations and (dash) from the analytical solution under the Bourret approximation [Eq. (D3)]. Two standard deviations of the admittance fluctuations are considered: (black) $\sigma_\beta = 0.25 \operatorname{Re}\{\langle\beta\rangle\}$ and (gray) $\sigma_\beta = 0.25\langle\beta\rangle$.

- ¹M. Bérengier, B. Gauvreau, P. Blanc-Benon, and D. Juvé, “Outdoor sound propagation: A short review on analytical and numerical approaches,” *Acta Acust. united Acust.* **89**, 980–991 (2003).
- ²E. M. Salomons, *Computational Atmospheric Acoustics* (Kluwer Academic Publishers, Dordrecht, the Netherlands, 2001), pp. 1–335.
- ³T. van Renterghem, “Efficient outdoor sound propagation modeling with the finite-difference time-domain (FDTD) method: A review,” *Int. J. Aeroacoust.* **13**(5–6), 385–404 (2014).
- ⁴V. E. Ostashev and D. K. Wilson, *Acoustics in Moving Inhomogeneous Media*, 2nd ed. (CRC Press, Boca Raton, FL, 2016), Chaps. 10, 11, 12, and 13.
- ⁵B. Lihoreau, B. Gauvreau, M. Bérengier, P. Blanc-Benon, and I. Calmet, “Outdoor sound propagation modeling in realistic environments: Application of coupled parabolic and atmospheric models,” *J. Acoust. Soc. Am.* **120**(1), 110–119 (2006).
- ⁶D. Dragna, P. Blanc-Benon, and F. Poisson, “Impulse propagation over a complex site: A comparison of experimental results and numerical predictions,” *J. Acoust. Soc. Am.* **135**(3), 1096–1105 (2014).
- ⁷D. K. Wilson, E. L. Andreas, J. W. Weatherly, C. L. Pettit, E. G. Patton, and P. P. Sullivan, “Characterization of uncertainty in outdoor sound propagation predictions,” *J. Acoust. Soc. Am.* **121**(5), EL177–EL183 (2007).
- ⁸E. Brandão, A. Lenzi, and S. Paul, “A review of the *in situ* impedance and sound absorption measurement techniques,” *Acta Acust. united Acust.* **101**, 443–463 (2015).
- ⁹R. Kruse and V. Mellert, “Effect and minimization of errors in *in situ* ground impedance measurements,” *Appl. Acoust.* **69**, 884–890. (2008).
- ¹⁰D. Dragna, K. Attenborough, and P. Blanc-Benon, “On the inadvisability of using single parameter impedance models for representing the acoustical properties of ground surfaces,” *J. Acoust. Soc. Am.* **138**(4), 2399–2413 (2015).
- ¹¹G. Guillaume, O. Faure, B. Gauvreau, F. Junker, M. Bérengier, and P. L’Hermite, “Estimation of impedance model input parameters from *in situ* measurements: Principles and applications,” *Appl. Acoust.* **95**, 27–36 (2015).
- ¹²A. J. Cramond and C. G. Don, “Effects of moisture content on soil impedance,” *J. Acoust. Soc. Am.* **82**(1), 293–301 (1987).
- ¹³B. Gauvreau, “Long-term experimental database for environmental acoustics,” *Appl. Acoust.* **74**, 958–967 (2013).
- ¹⁴V. E. Ostashev, D. K. Wilson, and S. N. Vecherin, “Effect of randomly varying impedance on the interference of the direct and ground-reflected waves,” *J. Acoust. Soc. Am.* **130**(4), 1844–1850 (2011).
- ¹⁵J. G. Watson and J. B. Keller, “Reflection, scattering, and absorption of acoustic waves by rough surfaces,” *J. Acoust. Soc. Am.* **74**(6), 1887–1894 (1983).
- ¹⁶J. G. Watson and J. B. Keller, “Rough surface scattering via the smoothing method,” *J. Acoust. Soc. Am.* **75**(6), 1705–1708 (1984).
- ¹⁷S. N. Chandler-Wilde and D. C. Hothersall, “Sound propagation above an inhomogeneous impedance plane,” *J. Sound Vib.* **98**(4), 475–494 (1985).
- ¹⁸U. Frisch, “Wave propagation in random media,” in *Probabilistic Methods in Applied Mathematics*, edited by A. T. Bharucha-Reid (Academic Press Inc., London, UK, 1968), pp. 75–198.
- ¹⁹V. I. Tatarskii, *The Effects of the Turbulent Atmosphere on Wave Propagation* (Israel Program for Scientific Translation, Jerusalem, Israel, 1971), Chap. 5, pp. 335–364.
- ²⁰S. M. Rytov, Y. A. Kravtsov, and V. I. Tatarskii, *Principles of Statistical Radiophysics. Part 4, Wave Propagation Through Random Media*, 2nd ed. (Springer, Berlin, 1989), pp. 139–141.
- ²¹A. Derode, V. Mamou, and A. Tourin, “Influence of correlations between scatterers on the attenuation of the coherent wave in a random medium,” *Phys. Rev. E* **74**, 036606 (2006).
- ²²O. Faure, B. Gauvreau, F. Junker, P. Lafon, and C. Bourlier, “Modelling of random ground roughness by an effective impedance and application to time-domain methods,” *Appl. Acoust.* **119**, 1–8 (2017).
- ²³A. Ishimaru, J. D. Rockway, Y. Kuga, and S.-W. Lee, “Sommerfeld and Zenneck wave propagation for a finitely conducting one-dimensional rough surface,” *IEEE Trans. Antennas Propag.* **48**(9), 1475–1484 (2000).
- ²⁴S. F. Chien and W. W. Soroka, “Sound propagation along an impedance plane,” *J. Sound Vib.* **43**(1), 9–20 (1975).
- ²⁵L. M. Brekhovskikh and O. A. Godin, *Acoustics of Layered Media II*, 2nd ed. (Springer-Verlag, Berlin, 1999), Appendix A.3, formula A.3.4.

- ²⁶E. J. Brambley and G. Gabard, "Reflection of an acoustic line source by an impedance surface with uniform flow," *J. Sound Vib.* **333**(21), 5548–5565 (2014).
- ²⁷K. Attenborough, K. M. Li, and K. Horoshenkov, *Predicting Outdoor Sound* (Taylor & Francis, London, 2007) Chap. 2, p. 42.
- ²⁸D. Dagna and P. Blanc-Benon, "Physically admissible impedance models for time-domain computations of outdoor sound propagation," *Acta Acust. united Acust.* **100**(3), 401–410 (2014).
- ²⁹M. Bérengier, M. R. Stinson, G. A. Daigle, and J. F. Hamet, "Porous road pavements: Acoustical characterization and propagation effects," *J. Acoust. Soc. Am.* **101**(1), 155–162 (1997).
- ³⁰D. Dagna, P. Blanc-Benon, and F. Poisson, "Time-domain solver in curvilinear coordinates for outdoor sound propagation over complex terrain," *J. Acoust. Soc. Am.* **133**(6), 3751–3763 (2013).
- ³¹C. Bogey and C. Bailly, "A family of low dispersive and low dissipative explicit schemes for noise computation," *J. Comput. Phys.* **194**(1), 194–214 (2004).
- ³²L. Ehrhardt, S. Cheinet, D. Juvé, and P. Blanc-Benon, "Evaluating a linearized Euler equations model for strong turbulence effects on sound propagation," *J. Acoust. Soc. Am.* **133**(4), 1922–1933 (2013).
- ³³R. Troian, D. Dagna, C. Bailly, and M.-A. Galland, "Broadband liner impedance education for multimodal acoustic propagation in the presence of a mean flow," *J. Sound Vib.* **392**, 200–216 (2017).
- ³⁴K. U. Ingard and G. C. Maling, "On the effect of atmospheric turbulence on sound propagated over ground," *J. Acoust. Soc. Am.* **35**(7), 1056–1058 (1963).
- ³⁵P. Chevret, P. Blanc-Benon, and D. Juvé, "A numerical model for sound propagation through a turbulent atmosphere near the ground," *J. Acoust. Soc. Am.* **100**(6), 3587–3599 (1996).
- ³⁶M. J. M. Martens, L. A. M. van der Heijden, H. H. J. Walthaus, and W. J. J. M. van Rens, "Classification of soils based on acoustic impedance, air flow resistivity, and other physical soil parameters," *J. Acoust. Soc. Am.* **78**(3), 970–980 (1985).